

Large scale GW-BSE calculations with N^3 scaling: excitonic effects in dye sensitised solar cells

Margherita Marsili

Dipartimento di Fisica e Astronomia, Università di Padova, via Marzolo 8, I-35131 Padova, Italy

Edoardo Mosconi and Filippo De Angelis

Istituto CNR di Scienze e Tecnologie Molecolare, via Elce di Sotto 8, I-06123 Perugia, Italy and CompuNet, Istituto Italiano di Tecnologia, Via Morego 30, 16163 Genova, Italy.

Paolo Umari

Dipartimento di Fisica e Astronomia, Università di Padova, via Marzolo 8, I-35131 Padova, Italy

Excitonic effects due to electron-hole coupling play a fundamental role in renormalising energy levels in dye sensitised and organic solar cells determining the driving force for electron extraction. We show that first-principles calculations based on many-body perturbation theory within the GW-BSE approach provide a quantitative picture of interfacial excited state energetics in organic dye-sensitized TiO_2 , delivering a general rule for evaluating relevant energy levels. To perform GW-BSE calculations in such large systems we introduce a new scheme based on maximally localized Wannier's functions. With this method the overall scaling of GW-BSE calculations is reduced from $O(N^4)$ to $O(N^3)$.

I. INTRODUCTION

Excitonic effects due to electron-hole coupling play a fundamental role in renormalising energy levels in dye sensitised and organic solar cells determining the driving force for electron extraction. In particular, dye-sensitised solar cells (DSSCs)¹ are one of the most promising technologies for clean energy production. Although currently commercialized only for niche applications, they are important as prototypical cells sharing several features with organic and perovskite solar cells^{2,3}.

In DSSCs a semi-conducting oxide (typically meso or nano structured TiO_2) supports a layer of adsorbed dye molecules. The oxide is in contact with a transparent conductive oxide (TCO) and the dye molecules are in contact with a hole transporting medium which can be a polymeric solid or a redox couple in a liquid electrolyte (see Fig. 1). When a photon is adsorbed by the dye, one of its valence electrons is promoted to an empty level. Provided that its energy is higher than the TiO_2 conduction band minimum (CBM), it can be injected into the TiO_2 and travel towards the electrode leaving a hole in the dye. This can be eventually neutralised provided that its energy level is lower than that of the redox couple. Therefore the functioning of such a device crucially relies on the alignment among the energy levels of its components (Fig. 1). These refer to both charged excitations (as TiO_2 band edges) and neutral excitations (as the dye optical gap).

Density functional theory (DFT) is nowadays the standard approach for the modelling of complex systems as DSSCs providing an accurate description of the atomistic structure. Unfortunately, energy levels can be only approximately reproduced by DFT due to issues related to the well-known band-gap underestimation⁴.

Many-body perturbation theory approaches (MBPT)

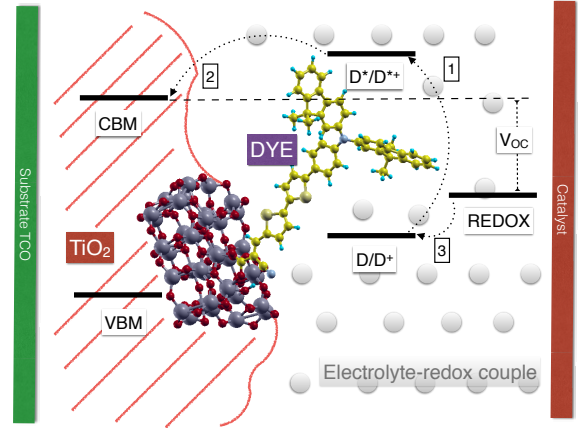


Figure 1: Schematic of a DSSC. The balls and sticks graph illustrates the atomic structure of the model TiO_2 cluster sensitised with the organic JK2 dye studied here. The main energy levels are: (D/D^+) dye ground state ionisation potential, (D^*/D^{++}) dye excited state ionisation potential, (CBM) TiO_2 conduction band minimum, (VBM) TiO_2 valence band maximum, (REDOX) level of the redox couple. V_{oc} is the open circuit voltage of the cell.

can overcome these issues⁵. Recently, the GW method^{6,7}, in which the electronic self-energy is expressed as the product of the one-particle Green's function G with the screened Coulomb interaction W , has been applied to models of DSSCs leading to the successful prediction of open-circuit voltages^{8,9}. However, the GW approach is appropriate only for the evaluation of charged excitations as it does not take into account electron-hole interactions. This is a major drawback for the calculation of the energy levels of the excited dye and even more severe for those of dye-sensitised semiconductors.

Electron-hole interactions are introduced into the first-principle MBPT framework through the Bethe Salpeter equation (BSE) approach which gives access to excitonic energies and amplitudes^{10,11}. However, the high computational cost of BSE approaches and in particular the N^4 scaling hinders their application to large model structures as those required for treating DSSCs. Methods presenting better N^3 scaling have been recently presented, however they are limited either to finite systems¹² or to a stochastic sampling of the response functions¹³.

Here, we introduce a general BSE method which allows much faster calculations on large systems thanks to a favorable N^3 scaling with respect to the system size. Indeed, we express the excitonic amplitudes as a set of excitations in correspondence with the maximally localised Wannier's functions¹⁴ which define the manifold of occupied states. In this way, we can avoid the calculation in the BSE equation of terms related to non-overlapping Wannier's functions, avoiding at the same time any explicit sum over empty one-particle DFT orbitals¹⁵. First, we validate our method addressing the relatively small C₆₀ molecule. Then, we apply it to a large model of a DSSC comprising the all-organic JK2¹⁶ dye adsorbed on a TiO₂ cluster.

II. METHOD

The MBPT formalism gives a BSE in which a Hamiltonian-like operator \hat{H}^{eh} accounts for the electron-hole interactions¹¹. Excitation energies Ω_S and amplitudes Θ are obtained solving:

$$\hat{H}^{eh} |\Theta\rangle = \Omega_S |\Theta\rangle \quad (1)$$

Within the Tamm-Dancoff approximation the many-body excitonic (excited) state $|\Theta\rangle$ is built starting from the ground state $|\Phi_0\rangle$ which is taken to be a single Slater determinant:

$$|\Phi_0\rangle = \frac{1}{\sqrt{N_v!}} \det |\psi_1 \dots \psi_{N_v}| \quad (2)$$

where N_v is the number of valence states. For simplicity we omit here spin indices. Spin multiplicity will be considered later. The one-body states ψ_i are the eigenstate of a Kohn-Sham Hamiltonian:

$$\epsilon_i^{KS} |\psi_i\rangle = H_{KS} |\psi_i\rangle \quad (3)$$

The GW method in its diagonal approximation is then used to obtain for each ψ_i the corresponding quasi-particle energy ϵ_i . We write, using the second quantization framework:

$$|\Phi_0\rangle = \frac{1}{\sqrt{N_v!}} \left(\prod_v \hat{a}_v^\dagger \right) |0\rangle \quad (4)$$

and

$$|\Theta\rangle = \sum_{vc} A_{vc} \hat{a}_v \hat{a}_c^\dagger |\Phi_0\rangle \quad (5)$$

where \hat{a}_i and \hat{a}_i^\dagger are the annihilation and construction operators for the i -th state, and the v and c indices run over the occupied and empty states, respectively. We define^{15,17}:

$$\xi_v(\mathbf{x}) = \sum_c A_{vc} \psi_c(\mathbf{x}) \quad (6)$$

where \mathbf{x} is a combined spin and position coordinate. In this way we can represent a generic excited state with N_v ξ_v functions which are represented in the code in the same way as wavefunctions with just the restriction of belonging to the manifold of empty KS states.

Instead of working with the KS valence states it can be convenient to work with their representation as maximally localised Wannier's functions $\{w_v\}$ ¹⁴:

$$w_v = \sum_{v'} U_{vv'} \psi_{v'} \quad (7)$$

where U is an unitary matrix:

$$\psi_v = \sum_{v'} U_{vv'}^{-1} w_{v'} = \sum_{v'} U_{v'v}^* w_{v'} \quad (8)$$

We can now express the excitonic state as:

$$|\Theta\rangle = \sum_v \left[\hat{a}_v \sum_c \left(\langle \psi_c | \tilde{\xi}_v \rangle \hat{a}_c^\dagger \right) \right] |\Phi_0\rangle \quad (9)$$

with the definitions:

$$\hat{a}_v = \left[\int d\mathbf{x} \hat{\Psi}(\mathbf{x}) w_v(\mathbf{x}) \right] = \sum_{v'} U_{vv'} \hat{a}_{v'} \quad (10)$$

and

$$\tilde{\xi}_v = \sum_{v'} U_{vv'}^* \xi_{v'} \quad (11)$$

In the following, we will focus on the general case of time-reversal symmetric systems. In this case the one-body states ψ_i and the U matrix can be taken real and we will omit in the following complex-conjugate signs. It is worth noting how the introduced transformation for the ξ_v 's works on the spatial representation $\Theta(\mathbf{x}, \mathbf{x}')$ of the excitonic state:

$$|\Theta\rangle = \int d\mathbf{x} d\mathbf{x}' \hat{\Psi}(\mathbf{x}) \hat{\Psi}^\dagger(\mathbf{x}') \Theta(\mathbf{x}, \mathbf{x}') \quad (12)$$

with:

$$\Theta(\mathbf{x}, \mathbf{x}') = \sum_{vc} \psi_v(\mathbf{x}) \sum_c A_{vc} \psi_c(\mathbf{x}') = \sum_v \psi_v(\mathbf{x}) \xi_v(\mathbf{x}') \quad (13)$$

it results:

$$\Theta(\mathbf{x}, \mathbf{x}') = \sum_v w_v(\mathbf{x}) \tilde{\xi}_v(\mathbf{x}') \quad (14)$$

We will now focus on the common case in which spin-orbit coupling can be neglected, we can separate spatial and spin coordinates and the ground state $|\Phi_0\rangle$ is built from N_v doubly occupied KS states. In this case the eigen-states of \hat{H}^{eh} will be either spin-singlet or spin-triplet states. In this case it is convenient to retain in the description of the excitonic state only the spatial coordinates. A generic excitonic states will be described by a set of N_v $\{\xi_v(\mathbf{r})\}$ functions. The \hat{H}^{eh} operator acting on these states involves only spatial coordinates but assumes a different form for spin-singlet and spin-triplet states:

$$\hat{H}_{singlet}^{eh} = \hat{D} + 2\hat{K}^x + \hat{K}^d \quad (15)$$

$$\hat{H}_{triplet}^{eh} = \hat{D} + \hat{K}^d \quad (16)$$

where \hat{D} is referred to as the diagonal operator, \hat{K}^x as the exchange one and \hat{K}^d as the direct one.

We show now how these operators act on the $\{\xi_v(\mathbf{r})\}$ and $\{\tilde{\xi}_v(\mathbf{r})\}$ representations of the excitonic state which we indicate using the bra-ket form as $|\{\xi\}\rangle$ and $|\{\tilde{\xi}\}\rangle$ ¹⁵. We start from the diagonal term \hat{D} in the A_{vc} representation :

$$A'_{vc} = \sum_{v'c'} D_{vc,v'c'} A_{v'c'} \quad (17)$$

with:

$$D_{vc,v'c'} = (\epsilon_c - \epsilon_v) \delta_{v,v'} \delta_{c,c'} \quad (18)$$

and we can write:

$$|\{\xi'\}\rangle = \hat{D} |\{\xi\}\rangle \quad (19)$$

with

$$|\xi'_v\rangle = (\hat{H}^{q.p.} - \epsilon_v) |\xi_v\rangle \quad (20)$$

where we suppose that the quasi-particle energies ϵ_i are given by the eigen-values of the Hamiltonian operator $\hat{H}^{q.p.}$ whose eigenfunctions coincide with the KS states

as we are using the diagonal GW approximation. Usually such an operator can be obtained from the Kohn-Sham Hamiltonian H_{KS} adding one or more scissor terms. It is worth noting that the $\{\xi'_v\}$ functions remain confined on the manifold of unoccupied KS states. The computational cost of applying the \hat{D} operator to a generic state $|\{\xi\}\rangle$ scales as $N^2 \log N$ with respect to the generic system size N . Indeed, applying the $\hat{H}^{q.p.}$ operator to a single ξ_v function has the same $N \log N$ scaling of applying a KS Hamiltonian while the number N_v of valence states scales as N .

For the \hat{K}^x operator acting on the $|\{\xi\}\rangle$ representation of an excitonic state, we start from the A_{vc} representation:

$$K_{vc,v'c'}^x = \int \psi_v(\mathbf{r}) \psi_c(\mathbf{r}) v(\mathbf{r}, \mathbf{r}') \psi_{v'}(\mathbf{r}') \psi_{c'}(\mathbf{r}') d\mathbf{r} d\mathbf{r}' \quad (21)$$

where v is the bare Coulomb operator (we recall that we consider real wavefunctions). We can write for :

$$|\{\xi'\}\rangle = \hat{H}^x |\{\xi\}\rangle \quad (22)$$

$$\xi'_v(\mathbf{r}) = \int P_c(\mathbf{r}, \mathbf{r}') \psi_v(\mathbf{r}') v(\mathbf{r}', \mathbf{r}'') \psi_{v'}(\mathbf{r}'') \xi_{v'}(\mathbf{r}'') d\mathbf{r}' d\mathbf{r}'' \quad (23)$$

where we used the projector operator on the manifold of unoccupied one-body states:

$$P(\mathbf{r}, \mathbf{r}') = \sum_c \psi_c(\mathbf{r}) \psi_c(\mathbf{r}') = \delta(\mathbf{r} - \mathbf{r}') - \sum_v \psi_v(\mathbf{r}) \psi_v(\mathbf{r}') \quad (24)$$

Hence, the evaluation of the $\{\xi'_v\}$ in Eq. 24 does not require the calculation of any unoccupied one-body state. The computational cost of applying the \hat{H}^x operator to a generic state $|\{\xi\}\rangle$ scales as N^3 . Indeed, the evaluation of the function:

$$\rho'(\mathbf{r}) = \sum_v \psi_v(\mathbf{r}) \xi_v(\mathbf{r}) \quad (25)$$

scales as N^2 and applying the \hat{P}_c projector to a single function scales as N^2 .

We show now how the \hat{K}^d operator acts on the $|\{\xi\}\rangle$ representation of an excitonic state. We start from the A_{vc} representation :

$$K_{vc,v'c'}^d = - \int \psi_c(\mathbf{r}) \psi_{c'}(\mathbf{r}) W(\mathbf{r}, \mathbf{r}') \psi_{v'}(\mathbf{r}') \psi_v(\mathbf{r}') d\mathbf{r} d\mathbf{r}' \quad (26)$$

where W is the static screened Coulomb interaction, and we write:

$$|\{\xi'\}\rangle = \hat{H}^d |\{\xi\}\rangle \quad (27)$$

$$\xi'_v(\mathbf{r}) = - \int P_c(\mathbf{r}, \mathbf{r}') \sum_{v'} \xi_{v'}(\mathbf{r}') \times \left[\int W(\mathbf{r}', \mathbf{r}'') \psi_{v'}(\mathbf{r}'') \psi_v(\mathbf{r}'') d\mathbf{r}'' \right] d\mathbf{r}'$$

with an overall computational cost scaling as N^4 due to the term in square brackets. In order to reduce the computational cost it is advantageous to turn to the Wannier's representation of the excitonic states:

$$\left| \left\{ \tilde{\xi}' \right\} \right\rangle = \hat{H}^d \left| \left\{ \tilde{\xi} \right\} \right\rangle \quad (28)$$

$$\tilde{\xi}'_v(\mathbf{r}) = - \int P_c(\mathbf{r}, \mathbf{r}') \sum_{v'} \tilde{\xi}_{v'}(\mathbf{r}') \times \left[\int W(\mathbf{r}', \mathbf{r}'') w_{v'}(\mathbf{r}'') w_v(\mathbf{r}'') d\mathbf{r}'' \right] d\mathbf{r}'$$

the computational cost can now be lowered to N^3 scaling if in the term in square brackets only terms involving overlapping couples of Wannier's functions are evaluated. Indeed, we neglect in the evaluation of \hat{K}^d the calculation of terms involving products of non-overlapping Wannier's functions and we indicate with s the threshold which determines whether two Wannier's function w_v and $w_{v'}$ overlap:

$$\int |w_v(\mathbf{r})|^2 |w_{v'}(\mathbf{r})|^2 d\mathbf{r} > s \quad (29)$$

The \hat{K}^d operator is usually separated into a bare $K^{d,b}$ and a correlation part $K^{d,c}$ according to the separation of the W operator as:

$$W(\mathbf{r}, \mathbf{r}') = v(\mathbf{r}, \mathbf{r}') + W_c(\mathbf{r}, \mathbf{r}') \quad (30)$$

where W_c is the correlation part of the screened Coulomb interaction. Let's inspect the first term:

$$\left| \left\{ \tilde{\xi}' \right\} \right\rangle = \hat{H}^{d,b} \left| \left\{ \tilde{\xi} \right\} \right\rangle \quad (31)$$

$$\tilde{\xi}'_v(\mathbf{r}) = - \int P_c(\mathbf{r}, \mathbf{r}') \sum_{v'} \tau_{vv'}^b(\mathbf{r}') \tilde{\xi}_{v'}(\mathbf{r}') d\mathbf{r}' \quad (32)$$

with:

$$\tau_{vv'}^b(\mathbf{r}) = \int v(\mathbf{r}, \mathbf{r}') w_{v'}(\mathbf{r}') w_v(\mathbf{r}') d\mathbf{r}' \quad (33)$$

which is evaluated only for overlapping couples v, v' of Wannier's functions. Let's inspect the second term:

$$\left| \left\{ \tilde{\xi}' \right\} \right\rangle = \hat{H}^{d,c} \left| \left\{ \tilde{\xi} \right\} \right\rangle \quad (34)$$

$$\tilde{\xi}'_v(\mathbf{r}) = - \int P_c(\mathbf{r}, \mathbf{r}') \tau_{vv'}^c(\mathbf{r}') \tilde{\xi}_{v'}(\mathbf{r}') d\mathbf{r}' \quad (35)$$

with:

$$\tau_{vv'}^c(\mathbf{r}) = \int W_c(\mathbf{r}, \mathbf{r}') w_{v'}(\mathbf{r}') w_v(\mathbf{r}') d\mathbf{r}' \quad (36)$$

which is evaluated only for overlapping couples v, v' of Wannier's functions. In our present implementation, we express W_c starting from the screened polarisability operator Π , in the static approximation:

$$W_c(\mathbf{r}, \mathbf{r}') = \int v(\mathbf{r}, \mathbf{r}'') \Pi(\mathbf{r}'', \mathbf{r}''') v(\mathbf{r}''', \mathbf{r}') d\mathbf{r}'' d\mathbf{r}''' \quad (37)$$

and we use an *optimal basis set* $\{\Phi_\mu\}$ for representing Π ^{18,19}:

$$\Pi(\mathbf{r}, \mathbf{r}') = \sum_{\mu\nu} \Phi_\mu(\mathbf{r}) \Pi_{\mu\nu} \Phi_\nu(\mathbf{r}') \quad (38)$$

We can now write:

$$W_c(\mathbf{r}, \mathbf{r}') = \sum_{\mu\nu} (v\Phi_\mu)(\mathbf{r}) \Pi_{\mu\nu} (v\Phi_\nu)(\mathbf{r}') \quad (39)$$

with the notation:

$$(v\Phi_\mu)(\mathbf{r}) = \int d\mathbf{r}' v(\mathbf{r}, \mathbf{r}') \Phi_\mu(\mathbf{r}') \quad (40)$$

We express the $\tau_{vv'}^c$ terms as:

$$\tau_{vv'}^c(\mathbf{r}) = \sum_{\mu} (v\phi_\mu)(\mathbf{r}) Z_{v'\mu}^v \quad (41)$$

with the definition:

$$Z_{v'\mu}^v = \sum_{\nu} \Pi_{\mu\nu} \int d\mathbf{r} (v\phi_\nu)(\mathbf{r}) w_v(\mathbf{r}) w_{v'}(\mathbf{r}) \quad (42)$$

We have implemented our method as a module of the Quantum-Espresso (Q-E) DFT package²⁰ which is based on the plane-waves pseudopotentials paradigm. We sample the Brillouin's zone at the sole Γ point and we can treat both extended (through periodic boundary conditions) and isolated systems. Quasi-particle energies are taken from a GW calculation for a set of conduction and valence states while for the residual states we apply to the DFT ones a scissor operator¹⁵. The static screened Coulomb interaction is provided by a GW calculation performed with the GWL code which overcomes the problem of sums over empty states^{18,19}. Maximally localised Wannier's function are obtained using the algorithm described in Ref.²¹. Single excitonic states can be calculated through a conjugate gradient minimization while the complex dielectric function can be directly evaluated through a Lanczos series²².

s (a.u.)	#Products	E_g (eV)
2500	90	3.67
500	180	1.86
50	900	1.87
5	2820	1.90
0.5	6816	1.92
0.05	11524	1.92
0.	14400	1.92

Table I: Optical band gap for C_{60} for various s thresholds with corresponding number of Wannier’s functions products.

III. VALIDATION

First, we validated our method considering the isolated benzene molecule comparing the first excitonic energies with those calculated with the Yambo code²³ starting from the same Q-E DFT. We find that values from the two calculations agree within 0.1 eV. As our implementation, but the $O(N^3)$ scaling due to the Wannier’s representation of excitonic amplitudes, is equivalent to ordinary plane-waves pseudo-potential BSE codes, the same good quality of results is expected for generic systems.

We then applied our BSE scheme to address the isolated C_{60} molecule. We take the atomic coordinates from Ref.²⁴ and choose the PBE exchange and correlation functional²⁵ for the starting DFT calculation together with a norm-conserving pseudo-potential²⁶. The cubic simulation cell has an edge of 40 Bohr and the Coulomb interaction is truncated at 20 Bohr. In Ref.²⁴ we investigated the GW quasi-particle energy levels finding a self-consistent HOMO-LUMO (electronic) gap of 4.94 eV (1.78 eV at the PBE level) and we consider the corresponding scissor operator in the BSE calculation. A basis of 2000 elements is used for representing the static polarisability operator^{18,19}.

For evaluating the C_{60} optical band gap, we obtained the lowest in energy optically allowed singlet exciton energy and the corresponding amplitude through a conjugate gradient minimisation. While, for evaluating optical absorption spectra, we obtained the complex dielectric susceptibility function through the Lanczos algorithm. As C_{60} exhibits 120 doubly occupied valence states the maximum number of product terms is 14400. In Tab. I, we report the calculated values for the optical gap as a function of the s threshold.

We observed that a large threshold s of 500 a.u., corresponding to only 180 product terms, was sufficient for converging the optical gap E_g within 0.06 eV with respect to the final value of 1.92 eV. This is in excellent agreement with the experimental figures of 1.92 eV (solution) and of 1.87 eV (bulk solid)²⁷ and with a previous BSE value of 1.88 eV²⁸. The same fast convergence with s is observed for the optical absorption spectrum reported in Fig. 2. Also in this case a threshold $s = 500$ a.u. yields results close (within 0.1 eV for peak positions) to

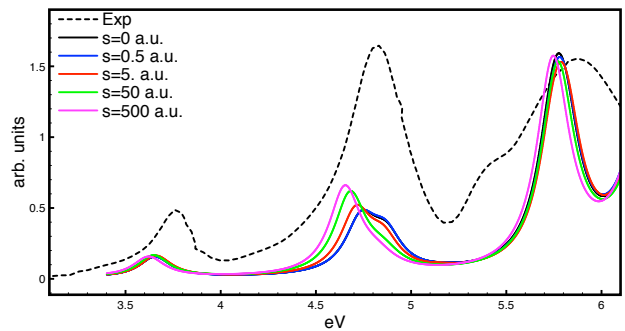


Figure 2: Optical absorption spectrum of molecular C_{60} : Experiment from Ref.²⁹ (black-dashed); GW-BSE (solid) with: $s = 0$ a.u. (black), $s = 0.5$ a.u. (blue), $s = 5$ a.u. (red), $s = 50$ a.u. (green), $s = 500$ a.u. (magenta). A Lorentzian broadening of 0.1 eV has been applied.

the fully-converged $s = 0$ a.u. calculation involving all possible product terms. We notice also good agreement with experimental data in solution²⁹ for the position and relative intensities of the main features.

IV. APPLICATION TO JK2@TiO₂

We can now apply our GW-BSE approach for evaluating the key energy levels in a DSSC model. We considered the same JK2@TiO₂ model structure of Ref.³⁰ exhibiting a dye molecule adsorbed on an anatase TiO₂ cluster (32 TiO₂ units) comprising 204 atoms and 1174 valence electrons in a $35 \times 35 \times 66.5$ Bohr³ periodic orthorhombic simulation cell. DFT calculations are performed using the BLYP exchange and correlation functional³¹ and wavefunctions are expanded on a plane waves basis set defined by a cutoff energy of 150 Ry. For the GW and the BSE calculations the polarisability operators are expanded on a (minimal) optimal basis set¹⁹ comprising 2500 vectors corresponding to an estimated accuracy for the GW energy levels of ~ 0.2 eV³². The BSE calculation has been performed using thresholds down to $s = 10$ a.u. The optical gap E_{gap} is determined through the position of the first peak in the calculated optical absorption spectrum consistently with the reported experimental data. In Tab. II we show that a threshold $s = 500$ a.u. assures convergence within ~ 0.1 eV as in the case of C_{60} involving only 2295 product terms to be contrasted to the total number of possible product terms $562^2 = 315844$. The same degree of accuracy is found for the absorption spectrum as displayed in Fig. 3.

In analogy with Refs.^{8,9}, the dye D/D⁺ level (neglecting any structural relaxation) is given by the uppermost occupied GW energy level with dye character which corresponds also to the HOMO of the entire JK2@TiO₂ system. The D^{*}/D⁺⁺ level is the excited state ionisation potential of the adsorbed dye which can be obtained from the D/D⁺ level adding the BSE lowest bright (singlet) excitation energy of the adsorbed dye. The evaluation

s (a.u.)	#Products	E_g (eV)	Tot. Time (s)	Time K^x (s)	Time K^d (s)	Single K^d (s)
500	2295	2.40	254580	43902	53079	23.1
50	7653	2.43	316082	43677	116256	15.2
10	12711	2.47	411780	44024	208490	16.4

Table II: GW-BSE calculations of the JK2@TiO₂ system for different values of the threshold s : number of Wannier's functions products (#Products), optical band gap (E_g); calculation times³³: total (Tot. time), for the exchange term K^x (Time K^x), for the direct term K^d (Time K^d), ratio Time K^d / #Products (Single K^d)

	Exp (eV)	GW-BSE (eV)
D/D ⁺ (eV)	-5.4	-5.9 (-5.8)
CBM	-4.0	-4.3 (-4.1)
E_{gap} (eV)	2.7	2.5 (2.5)

Table III: Energy levels for the JK2@TiO₂ system: D/D⁺ ground state dye ionisation potential, CBM TiO₂ conduction band minimum, E_{gap} optical gap. Experimental figure are from Ref.¹⁶. GW-BSE figures in parentheses: including solvent effects.

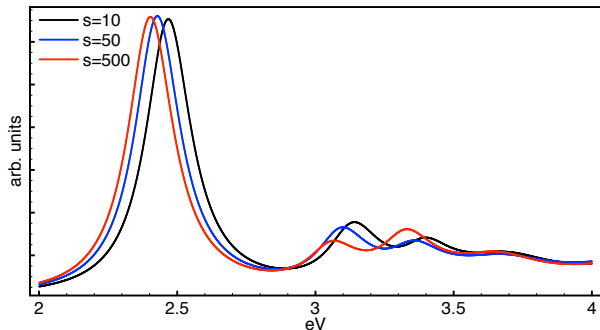


Figure 3: Optical absorption spectrum for the JK2@TiO₂ model: GW-BSE with: $s = 10$ a.u. (black), $s = 50$ a.u. (blue), $s = 500$ a.u. (red). A Lorentzian broadening of 0.1 eV has been applied.

of the TiO₂ CBM is more delicate. Indeed, the electronic VBM-CBM gap converges very slowly towards the bulk value when calculated on slabs or clusters of increasing size. Moreover, this issue is more severe for the GW approach³⁵. However, we previously found that the absolute position of the VBM in anatase TiO₂ slabs converges faster with respect to slab width and is in agreement with available experimental data³⁶. This is related to the localisation of the manifold of occupied states. Hence, a good estimate for the TiO₂ CBM can be obtained by adding to the VBM value, calculated for the cluster, the electronic band gap of bulk anatase TiO₂ from an equivalent GW calculation for a bulk model structure (3.6 eV⁸).

As displayed in Tab. III the GW-BSE energy levels are in a quite good agreement with experiment even without considering any solvent effect. These can be estimated considering the shift of the energy levels at the sole DFT BLYP level using an implicit solvent model. This further increases the quality of the GW-BSE results showing

that the GW-BSE approach can predict at the same time both charged and neutral energy levels. We note that our GW-BSE results improve on the best TD-DFT ones presented in Ref.³⁰ for the same JK2@TiO₂ system which strongly depend on the flavour of the adopted hybrid exchange and correlation functional. We don't have such arbitrariness in BSE as such method as been shown to give good results both for isolated and extended systems in contrast to what is recorded for TD-DFT.

V. CONCLUSIONS

It is worth stressing that with our method a BSE calculation performed on a large system as JK2@TiO₂ was made possible even with quite restricted computational resources³³. Indeed, for this system the total number of possible Wannier's functions products is huge (344569). In Fig. 3 and Tab. II, we show that only a fraction of these products is required for assuring good convergence while the cost for evaluating the K^d term of the excitonic Hamiltonian scales almost linearly with such number³⁴. Indeed, a threshold $s = 500$ a.u., corresponding to ~ 4 product terms for each Wannier's function, leads to pretty well converged results. Considering all the possible Wannier's functions products would require a ~ 150 times longer computation together with much more severe requirements in terms of memory usage.

We note that a constant number of product terms for each Wannier's function determines a theoretical $O(N^3)$ scaling based on the computational cost of the terms appearing in the excitonic Hamiltonian. We checked that this relation is observed when comparing two analogous C₆₀ and JK2@TiO₂ BSE Lanzos (200 steps) calculations for the same $s = 500$ a.u. threshold which gives comparable accuracy. The theoretically expected cost of the JK2@TiO₂ (T_{JK2}^*) calculation can be obtained from the computing time of the C₆₀ one (T_{C60}):

$$T_{JK2}^* = \left(\frac{N_{\text{cores}}^{JK2}}{N_{\text{cores}}^{C60}} \right) \left(\frac{N_{PW}^{JK2}}{N_{PW}^{C60}} \right) \left(\frac{N_v^{JK2}}{N_v^{C60}} \right)^3 T_{C60},$$

where N_{core} is the number of used computing cores, N_v the number of valence states, and N_{PW} the ratio between number of plane waves and of valence states. The $(N_{PW}^{JK2}/N_{PW}^{C60})$ ratio must be added because of the different energy cutoffs used in C₆₀ and in JK2@TiO₂ for

defining the plane waves basis sets: 45 and 150 Ry, respectively. The relevant figures for C_{60} are: $N_{\text{cores}}^{C_{60}} = 32$, $N_{PW}^{C_{60}} = 2716$, and $T_{C_{60}} = 2070$ s. The corresponding figures for JK2@TiO₂ are: $N_{\text{cores}}^{JK2} = 64$, $N_{PW}^{JK2} = 4403$, and $T_{JK2} = 254580$ s. Hence, the estimated computing time found for JK2@TiO₂ is $T_{JK2}^* = 196395$ s, in excellent agreement with the recorded one (254580 s).

In conclusion, we presented a method which permits to extend the scope of state of the art BSE calculations even using limited computational resources. This is achieved by applying the unitary transformation, which defines maximally localised Wannier's functions of valence KS orbitals, to excitonic amplitudes. The accuracy is con-

trolled by a single parameter with a clear physical meaning (i.e. defining the overlap of Wannier's functions). Moreover, its formulation is general and can be extended towards other applications as TD-DFT. Further speed-up could be obtained restricting integrals in real space only to the volumes where Wannier's functions are not vanishing.

This permitted us to solve the problem of energy level alignment in JK2@TiO₂ opening the way to the use of BSE for addressing complex systems in the modelling of photovoltaics and optoelectronic materials where ordinary approaches fail.

-
- ¹ B. O'Regan and M. Grätzel, *Nature* 352, 737 (1991).
 - ² M.M. Lee, J. Teuscher, T. Miyasaka, T.N. Murakami, H.J. Snaith, *Science* 338, 643–647, (2012).
 - ³ J. Burschka, et al. *Nature* 499, 316–319, (2013).
 - ⁴ F. De Angelis, *Acc. Chem. Res.* 47, 3349 (2014).
 - ⁵ G. Onida, L. Reining, and A. Rubio *Rev. Mod. Phys.* 74, 601 (2002).
 - ⁶ L. Hedin, *Phys. Rev.* 139, A796 (1965)
 - ⁷ M.S. Hybertsen and S.G. Louie, *Phys. Rev. B* 34, 5390 (1986).
 - ⁸ P. Umari, L. Giacomazzi, F. De Angelis, M. Pastore, and S. Baroni, *J. Chem. Phys.* 139, 014709 (2013).
 - ⁹ C. Verdi, E. Mosconi, F. De Angelis, M. Marsili, and P. Umari, *Phys. Rev. B* 90, 155410 (2014).
 - ¹⁰ G. Strinati, *Riv. Nuovo Cimento* 11, 1 (1988).
 - ¹¹ M. Rohlfing and S. G. Louie, *Phys. Rev. B* 62, 4927 (2000).
 - ¹² M.P. Ljungberg, P.Koval, F.Ferrari, D.Foerster, and D. Sánchez-Portal, *Phys. Rev. B* 92, 075422 (2015).
 - ¹³ E. Rabani, R.Baer, D. Neuhauser, *Phys. Rev. B* 91, 235302 (2015).
 - ¹⁴ N. Marzari and D. Vanderbilt *Phys. Rev. B* 56, 12847 (1997).
 - ¹⁵ D. Rocca, D. Lu, and G. Galli, *J. Chem. Phys.* 133, 164109 (2010).
 - ¹⁶ S. Kim, J.K. Lee, S.O. Kang, J.Ko, J.H. Yum, S. Fantacci, F. DeAngelis, D. Di Censo, M.K. Nazeeruddin, M. Grätzel, *J.Am. Chem. Soc.* 128, 16701 (2006).
 - ¹⁷ B. Walker, A.M. Saitta, R. Gebauer, and S. Baroni, *Phys. Rev. Lett.* 96, 113001 (2006).
 - ¹⁸ P.Umari, G. Stenuit, and S. Baroni, *Phys. Rev. B* 79, 201104(R) (2009) .
 - ¹⁹ P.Umari, G. Stenuit, and S. Baroni, *Phys. Rev. B* 81, 115104 (2010).
 - ²⁰ P. Giannozzi, et al. *J. Phys. Condens. Matter* 21, 395502 (2009).
 - ²¹ F. Gygi, J-L. Fattebert, and E. Schwegler. *Comp. Phys. Comm.* 155, 1 (2003).
 - ²² A. L. Ankudinov, C. E. Bouldin, J. J. Rehr, J. Sims, and H. Hung *Phys. Rev. B* 65, 104107 (2002).
 - ²³ A. Marini, C. Hogan, M. Grüning, and D. Varsano *Comp. Phys. Comm.* 180, 1392 (2009).
 - ²⁴ X. Qian, P. Umari, and N. Marzari *Phys. Rev. B* 91, 245105 (2015).
 - ²⁵ J.P. Perdew, K. Burke, and M. Ernzerhof, *Phys. Rev. Lett.* 77, 3865 (1996).
 - ²⁶ We use the C.pbe-tm.UPF pseudo-potential from the Q-E repository.
 - ²⁷ Y. Wang, J. M. Holden, A. M. Rao, P. C. Eklund, U. D. Venkateswaran, D.L. Eastwood, R.L. Lidberg, G. Dresselhaus, and M.S. Dresselhaus, *Phys. Rev. B* 51, 4547 (1995).
 - ²⁸ M.L. Tiago, P.R.C. Kent, R.Q. Hood, and F. A. Reboredo, *J. Chem. Phys.* 129, 084311 (2008).
 - ²⁹ R. Bauernschmitt, R. Ahlrichs, F.H. Hennrich, and M.M. Kappes, *J. Am. Chem. Soc.* 120, 5052 (1998).
 - ³⁰ M. Pastore, S. Fantacci, and F. De Angelis, *J. Phys. Chem. C* 117, 3685 (2013).
 - ³¹ A. D. Becke, *Phys. Rev. A* 38, 3098 (1988); C. Lee, W. Yang, and R. G. Parr, *Phys. Rev. B* 37, 785 (1988).
 - ³² We applied a cutoff energy $E^* = 2$ Ry.
 - ³³ Calculations were run on an INTEL Xeon 2.6 GHz 64 cores computer cluster with 8GB RAM per core.
 - ³⁴ Computing K^d for a single Wannier's functions product is slightly longer for small and large s for the worse use of cache and swap memory, respectively.
 - ³⁵ C. Freysoldt, P. Eggert, P. Rinke, A. Schindlmayr, and M. Scheffler, *Phys. Rev. B* 77, 235428 (2008).
 - ³⁶ We repeated the calculations of Ref.⁸ with a dye@TiO₂ model comprising 3 TiO₂ layers instead of 2. The VBM changes of only +0.1 eV.